IEEE Photonics Journal
An IEEE Photonics Society Publication

Open Access

Continuously Tunable Flat-Passband Microwave Photonic Notch Filter Based on Primary and Secondary Tap Distribution Impulse Response

Volume 7, Number 1, February 2015

Y. Wang
E. H. W. Chan
X. Wang
X. Feng
B. Guan

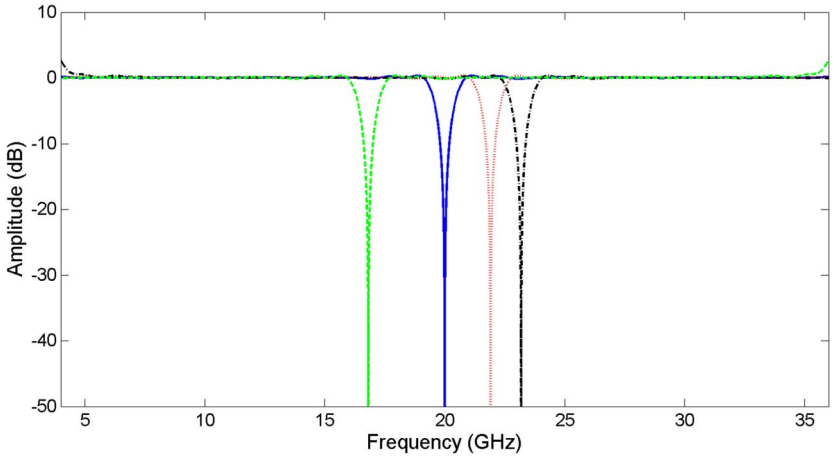

DOI: 10.1109/JPHOT.2015.2393874
1943-0655

IEEE photonics SOCIETY
IEEE

Continuously Tunable Flat-Passband Microwave Photonic Notch Filter Based on Primary and Secondary Tap Distribution Impulse Response

Y. Wang,[1] E. H. W. Chan,[2] X. Wang,[1] X. Feng,[1] and B. Guan[1]

[1]Institute of Photonics Technology, Jinan University, Guangzhou 510632, China
[2]School of Engineering and Information Technology, Charles Darwin University, Darwin, NT 0909 Australia

DOI: 10.1109/JPHOT.2015.2393874

Manuscript received December 18, 2014; revised January 12, 2015; accepted January 13, 2015. Date of publication January 19, 2015; date of current version February 10, 2015. This work was supported in part by the National Science Foundation of China under Grant 61475065, by the Natural Science Foundation of Guangdong Province of China under Grant S2012010008850, and by the Fundamental Research Funds for the Central Universities in China under Grant 21612201. Corresponding author: X. Wang (e-mail: txudong.wang@email.jnu.edu.cn).

Abstract: A new microwave photonic signal processor that has the ability to realize a continuously tunable high-resolution notch filter response is presented. It is based on designing the filter impulse response to have a primary and secondary tap distribution. With a proper design on the tap amplitudes, the notch filter passband can be flattened. The filter notch frequency can be also continuously tuned by controlling the phase shift of the secondary taps via a diffraction-based Fourier-domain optical processor. The notch filter has a robust response and high signal-to-noise-ratio (SNR) performance. Experimental results demonstrate that the new microwave photonic notch filter can simultaneously realize a flat passband of only a 1-dB ripple, a large free spectral range of 4.7 GHz, and a notch depth of over 40 dB while tuning the notch frequency.

Index Terms: Microwave photonics, optical signal processing, frequency response, notch filters.

1. Introduction

Processing microwave signals in the optical domain has the advantages of realizing extremely high multigigahertz sampling frequencies, high time-bandwidth product capabilities, immunity to electromagnetic interference, and compatibility with an optical fiber transport system [1]. It has applications in defense, radioastronomy, and next-generation wireless optical communication systems.

Notch filters are required in many systems to remove unwanted interfering signals. The important performance requirements for such filters to be used in the aforementioned applications are continuous notch frequency tunability, large operating bandwidth, flat passband, deep notch, and narrow 3-dB notch width to allow notch filtering without affecting the wanted information signals. Various microwave photonic techniques have been reported to implement a notch filter [2]–[11]. However, most of them are limited to only two taps [2]–[4] or just four taps [5]–[7], which produce a low-resolution notch filter response causing significant frequency-dependent

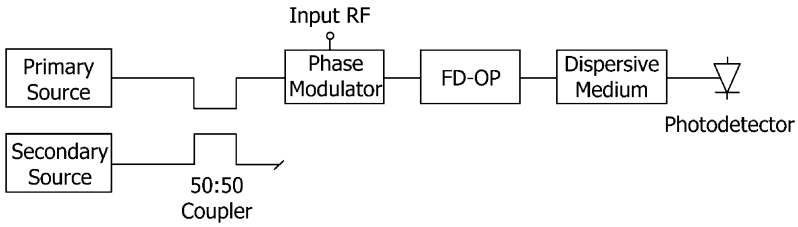

Fig. 1. Topology of the primary and secondary tap distribution based MPNF.

attenuation in the passband that affects the wanted information signals. A multiple wavelength optical signal remodulation technique has been proposed to realize a multiple-tap microwave photonic notch filter (MPNF) [8]. However, it has a limited free spectral range (FSR) due to the round-trip delay time cannot be made very small. Recently, a MPNF based on a high birefringence fiber Bragg grating based Fabry–Perot cavity has been reported [9]. It solves the limited FSR problem and demonstrates continuous notch frequency tuning, but the filter passband is not flat, and the passband amplitude changes while tuning the notch frequency. Stimulated Brillouin scattering (SBS) is a powerful technique for implementing a microwave photonic filter. A single-passband filter based on a vector SBS process has been reported [12]. The filter has a high out of band rejection of 30 dB and a narrow 3 dB bandwidth of $\sim$20 MHz. SBS can also be used to improve the shape factor performance of a microwave photonic channelizer [13]. The SBS based microwave photonic channelizer can be designed to have different bandwidth and different channel spacing with a shape factor below 2. The SBS based MPNFs [10], [11] can realize a large FSR continuously-tunable notch filter response with a flat passband. However, the SBS process is polarization dependent. Hence, the light polarization state needs to be carefully controlled or polarization maintaining components are required in the setup, which increase the system cost. Moreover they have a complex structure as two or more electro-optic modulators and a microwave signal generator are needed. Furthermore a recent study found that the frequency response shape of an SBS based microwave photonic filter is dependent on the input RF signal power. Though a technique has been proposed to ease the input RF signal power dependent frequency response problem but the problem remains unsolved [14]. Until now, there have been very few reports on continuously-tunable, large-FSR, flat-passband MPNFs.

In this paper, we present a continuously-tunable MPNF that can simultaneously realize a flat passband, a narrow notch width and a large FSR notch filter response with robust performance. It is based on designing the notch filter impulse response to have a primary and secondary tap distribution. The continuous notch frequency tuning operation is realized by controlling the phase of the optical carriers and RF modulation sidebands through a diffraction-based Fourier-domain optical processor (FD-OP). The FD-OP can also control the tap amplitude to flatten the notch filter passband. Experimental results are presented, which demonstrate a large FSR and flat passband notch filter response with continuous notch frequency tunability.

2. Topology and Principle of Operation

The primary and secondary tap distribution based MPNF is a multi-tap transverse filter with the amplitude and phase of the individual taps being controlled by a programmable spectral processor. Its topology is shown in Fig. 1. The optical source composes of a primary source and a secondary source. The primary source produces a single wavelength with high optical power. The secondary source produces multiple wavelengths with lower optical powers. The outputs of the primary and secondary sources are combined by a 50:50 optical coupler and are phase modulated by an input RF signal. The RF phase modulated optical signals are launched into an FD-OP, which is formed by a 2-D liquid crystal on silicon (LCoS) pixel array. It distributes the RF phase modulated optical signals to different locations on the LCoS array dependent on the wavelengths of the optical source [15]. The FD-OP has two functions in this MPNF. One is that it filters out one sideband of the phase modulated signal to realize single sideband modulation

to avoid the dispersion induced power fading problem [16]; another is that it controls both the amplitude and phase of the different-wavelength optical carriers and sidebands independently. This is done by programming the horizontal and vertical axis of the LCoS pixel panel. The multiple-wavelength Fourier-domain optical processed signals then pass through a dispersive medium to introduce delays between different wavelengths and are detected by a photodetector. Note that the phase modulator in Fig. 1 can be replaced by a single sideband (SSB) modulator formed by a 90 degree hybrid coupler and a DC bias voltage at the input of a dual drive Mach–Zehnder modulator. This enables the system to operate at a lower frequency. However, the SSB modulator has the bias drift problem, which requires a bias controller to stabilize the modulator bias point. Furthermore, the 90 degree hybrid coupler is an electrical component, which limits the notch filter bandwidth. Hence, SSB modulation implemented by using a FD-OP to filter out one sideband of the phase modulated optical signal is preferred.

Each wavelength from the optical source can generate one delayed optical signal or tap formed by the beating between the carrier and the corresponding sideband at the photodetector. The tap amplitude is proportional to the product of the corresponding carrier and sideband amplitudes. The phase shift of the tap equals to the phase difference between the carrier and the corresponding sideband. A notch filter response can be obtained by designing the tap amplitudes and separations. This requires the amplitude of the primary tap, generated by the primary source, equals to the sum of amplitudes of the secondary taps, generated by the secondary source. The secondary taps are designed to have the same time delay τ except the first secondary tap, which needs to have 0.5τ time delay to the primary tap. Since the tap separation is proportional to the wavelength separation of each tap, the required tap time delay relationship can be obtained by using a dispersive medium and by controlling the wavelength separations of the optical sources. The required tap amplitude relationship can be obtained by controlling the optical power of the primary and secondary source and by programming the carrier and the sideband amplitude for each tap via the FD-OP. The resolution of the notch filter is dependent on the number of secondary taps, which in turn depends on the number of wavelengths generated by the secondary source. Various techniques such as spectrum slicing a broadband optical source, the multiwavelength erbium-doped fiber laser [17], or wide-band parametric frequency comb generator [18], can be used to generate many secondary wavelengths to realize a high-resolution notch filter response. Since the tap separation is proportional to the wavelength separation and the dispersion parameter of the dispersive medium, which can be made small, the structure has the ability to realize a large FSR frequency response. It should be noted that the ability of independently controlling the amplitude and the phase shift of each tap enables a highly reconfigurable notch filtering operation to be realized.

3. Analysis and Simulation Results

Assume that the optical source consists of the primary source with the optical carrier frequency of ω_P and the secondary source with N optical carrier frequencies of $\omega_{S,1}$ to $\omega_{S,N}$. The electric field at the output of the optical phase modulator can be expressed as

$$E(t) = \frac{\sqrt{2}}{2} E_P \sqrt{t_{ff}} [J_0(\beta_{\mathrm{RF}}) \exp j(\omega_P) t - J_1(\beta_{\mathrm{RF}}) \exp j(\omega_P - \omega_{\mathrm{RF}}) t + J_1(\beta_{\mathrm{RF}}) \exp j(\omega_P + \omega_{\mathrm{RF}}) t] + \frac{\sqrt{2}}{2} \sum_{n=1}^{N} E_{S,n} \sqrt{t_{ff}} [J_0(\beta_{\mathrm{RF}}) \exp j(\omega_{S,n}) t - J_1(\beta_{\mathrm{RF}}) \exp j(\omega_{S,n} - \omega_{\mathrm{RF}}) t + J_1(\beta_{\mathrm{RF}}) \exp j(\omega_{S,n} + \omega_{\mathrm{RF}}) t] \quad (1)$$

where E_P and $E_{S,n}$ are the electric field amplitude of the primary source and the nth wavelength in the secondary source at the input of the phase modulator respectively, t_{ff} is the phase modulator insertion loss, $J_m(x)$ is the Bessel function of mth order of first kind, $\beta_{\mathrm{RF}} = \pi V_{\mathrm{RF}} / V_\pi$ is the modulation index, V_{RF} is the modulator input RF signal amplitude, V_π is the switching voltage of the optical phase modulator, and ω_{RF} is the input RF signal angular frequency. The FD-OP is

programmed to remove the lower sideband of the RF phase modulated optical signal, to introduce a phase shift to the carrier and the upper sideband, and to control the carrier and the upper sideband amplitudes, as was discussed in the previous section. The electric field at the FD-OP output can be expressed as

$$E(t) = \frac{\sqrt{2}}{2} E_P \sqrt{t_{ff}} [\sqrt{\alpha_{cP}} J_0(\beta_{\mathrm{RF}}) \exp j(\omega_P t + \phi_{cP}) + \sqrt{\alpha_{sP}} J_1(\beta_{\mathrm{RF}}) \exp j((\omega_P + \omega_{\mathrm{RF}})t + \phi_{sP})] + \frac{\sqrt{2}}{2} \sum_{n=1}^{N} E_{S,n} \sqrt{t_{ff}} [\sqrt{\alpha_{cS,n}} J_0(\beta_{\mathrm{RF}}) \exp j(\omega_{S,n} t + \phi_{cS,n}) + \sqrt{\alpha_{sS,n}} J_1(\beta_{\mathrm{RF}}) \exp j\big((\omega_{S,n} + \omega_{\mathrm{RF}})t + \phi_{sS,n}\big)] \quad (2)$$

where α_{cP} and α_{sP} are the power attenuation of the primary source carrier and upper sideband introduced by the FD-OP, respectively, $\alpha_{cS,n}$ and $\alpha_{sS,n}$ are the power attenuation of the nth wavelength of the secondary source carrier and upper sideband respectively, ϕ_{cP} and ϕ_{sP} are the phase of the primary source carrier and upper sideband introduced by the FD-OP, respectively, and $\phi_{cS,n}$ and $\phi_{sS,n}$ are the phase of the nth wavelength of the secondary source carrier and upper sideband, respectively.

The time delay introduced by the dispersive medium is proportional to the wavelength separation of the optical source. The separations of all the secondary source wavelengths are equal. The separation between the primary source wavelength and the first wavelength of the secondary source is half of the secondary source wavelength separation. Therefore the time delay between the primary wavelength to the nth secondary wavelength is $(\mathrm{n} - 0.5)\tau$. The electric field after the dispersive medium can be written as

$$E(t) = \frac{\sqrt{2}}{2} E_P \sqrt{t_{ff}} [\sqrt{\alpha_{cP}} J_0(\beta_{\mathrm{RF}}) \exp j(\omega_P t + \phi_{cP}) + \sqrt{\alpha_{sP}} J_1(\beta_{\mathrm{RF}}) \exp j((\omega_P + \omega_{\mathrm{RF}})t + \phi_{sP})] + \frac{\sqrt{2}}{2} \sum_{n=1}^{N} E_{S,n} \sqrt{t_{ff}} \left[\sqrt{\alpha_{cS,n}} J_0(\beta_{\mathrm{RF}}) \exp j\left(\omega_{S,n}\left(t + \left(n - \frac{1}{2}\right)\tau\right) + \phi_{cS,n}\right) + \sqrt{\alpha_{sS,n}} J_1(\beta_{\mathrm{RF}}) \exp j\left((\omega_{S,n} + \omega_{\mathrm{RF}})\left(t + \left(n - \frac{1}{2}\right)\tau\right) + \phi_{sS,n}\right)\right]. \quad (3)$$

Assuming the separation of the optical source wavelength is wide enough so that the photodetector only detects the beating of the carrier and its sideband. The optical power into the photodetector is the output electric field square. The optical power at the RF frequency is given by

$$P_{\mathrm{out}} = t_{ff} J_0(\beta_{\mathrm{RF}}) J_1(\beta_{\mathrm{RF}}) \sqrt{A^2 + B^2} \quad (4)$$

where

$$A = P_P \sqrt{\alpha_{cP}} \sqrt{\alpha_{sP}} \cos \Delta\phi_P + \sum_{n=1}^{N} P_{S,n} \sqrt{\alpha_{cS,n}} \sqrt{\alpha_{sS,n}} \cos \left[\omega_{\mathrm{RF}}\left(n - \frac{1}{2}\right)\tau + \Delta\phi_{S,n}\right] \quad (5)$$

$$B = P_P \sqrt{\alpha_{cP}} \sqrt{\alpha_{sP}} \sin \Delta\phi_P + \sum_{n=1}^{N} P_{S,n} \sqrt{\alpha_{cS,n}} \sqrt{\alpha_{sS,n}} \sin \left[\omega_{\mathrm{RF}}\left(n - \frac{1}{2}\right)\tau + \Delta\phi_{S,n}\right] \quad (6)$$

where P_P is the optical power of the primary source, $P_{S,n}$ is the optical power of the nth wavelength in the secondary source, $\tau = \Delta\lambda D$ is the basic time delay, $\Delta\lambda$ is the wavelength separation in the secondary source, D is the dispersion parameter (ps/nm) of the dispersive medium, and $\Delta\phi_P = \phi_{sP} - \phi_{cP}$ and $\Delta\phi_{S,n} = \phi_{sS,n} - \phi_{cS,n}$. Under the small signal condition, the filter power transfer function can be obtained from (4) and can be written as

$$|H(f_{\mathrm{RF}})|^2 = \frac{1}{4}\left(\frac{\pi}{V_\pi}\right)^2 R_{\mathrm{in}} R_o t_{ff}^2 \Re^2 (A^2 + B^2) \quad (7)$$

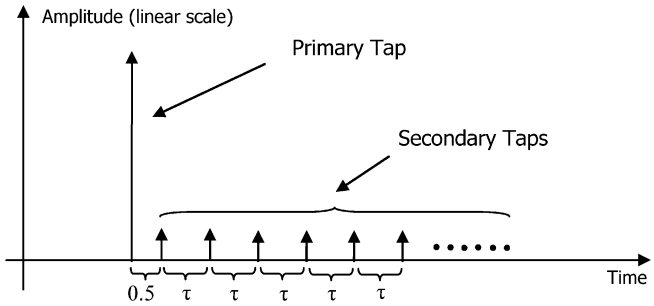

Fig. 2. Primary and secondary tap distribution based MPNF impulse response.

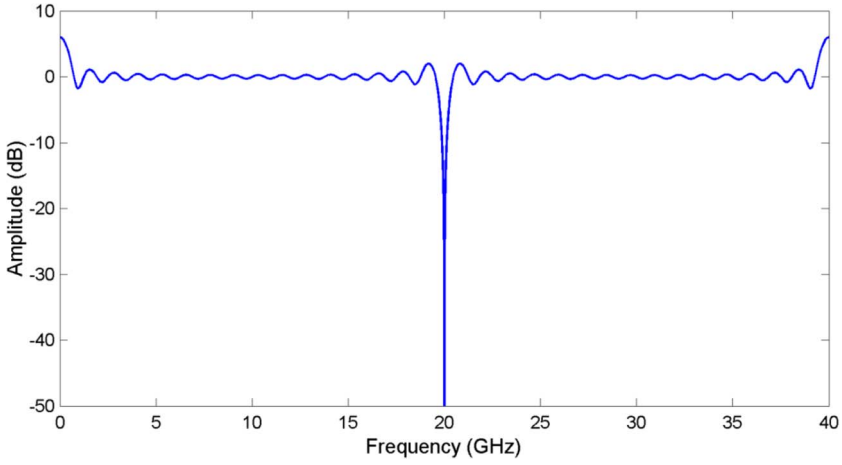

Fig. 3. Simulated frequency response of the primary and secondary tap distribution based MPNF with 16 secondary taps.

where $\mathcal{R}$ is the photodiode responsivity, R_{in} is the modulator input resistance, and R_o is the photodetector load resistance. In order to obtain a notch filter response with deep notch, the relationship of the primary and secondary tap amplitudes needs to be

$$P_P\sqrt{\alpha_{cP}}\sqrt{\alpha_{sP}} = \sum_{n=1}^{N} P_{S,n}\sqrt{\alpha_{cS,n}}\sqrt{\alpha_{sS,n}}. \tag{8}$$

The above analysis show the amplitude and phase of the primary tap are dependent on $P_P\sqrt{\alpha_{cP}}\sqrt{\alpha_{SP}}$ and $\Delta\phi_P$, respectively, and the amplitude and phase of the nth tap generated by the secondary source are dependent on $P_{S,n}\sqrt{\alpha_{cS,n}}\sqrt{\alpha_{sS,n}}$ and $\Delta\phi_{S,n}$, respectively. This indicates that the amplitude and phase of each tap can be controlled independently by programming the FD-OP. The MPNF impulse response is illustrated in Fig. 2. Note that all the taps have the same phase of 0°. The primary tap has the largest amplitude, which is equal to the sum of all the secondary tap amplitudes, and has a half time delay separation 0.5τ to the first secondary tap. All the secondary taps have the same amplitude and have the same time delay separation τ. The simulated frequency response of the primary and secondary tap distribution based MPNF with 16 secondary taps and 25 ps half time delay, which corresponds to an FSR of 40 GHz, is shown in Fig. 3.

It can be seen from the figure that the MPNF has a narrow notch with a 3-dB notch width of only 1.5% of the filter FSR. The figure shows the MPNF has 3 dB ripples at the passband. The filter passband ripple amplitude can be reduced by designing the secondary tap amplitude ratio so that the secondary taps have a decreasing taper as shown in Fig. 4. As an example the

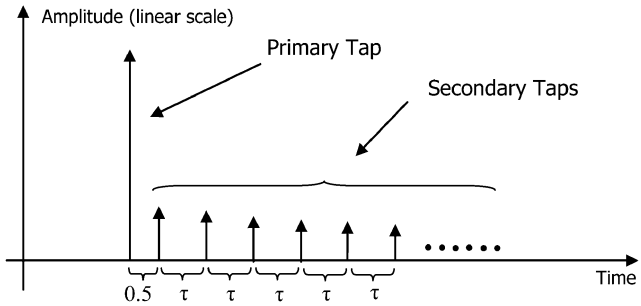

Fig. 4. Primary and secondary tap distribution based MPNF impulse response with a decreasing taper.

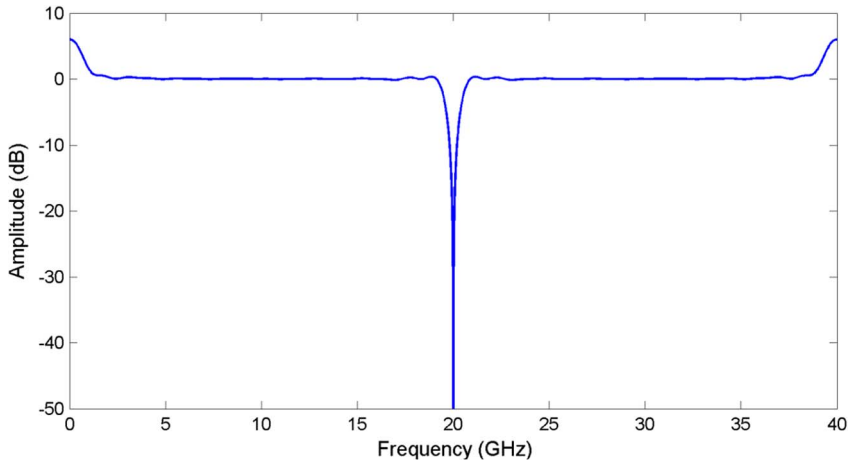

Fig. 5. Simulated frequency response of the primary and secondary tap distribution based MPNF with 16 secondary taps. The secondary tap amplitudes are optimized to minimize the filter passband ripples.

optimized secondary tap amplitude ratios of the primary and secondary tap distribution based MPNF with 16 secondary taps were found to be 1, 0.94, 0.87, 0.8, 0.75, 0.68, 0.62, 0.5, 0.4, 0.35, 0.25, 0.2, 0.15, 0.1, and 0.05. The primary tap amplitude ratio is 7.95, which is the sum of all the secondary tap amplitude ratios. The frequency response of the primary and secondary tap distribution based MPNF with the optimum tap amplitude ratios is shown in Fig. 5. It can be seen from the figure that the filter passband ripple amplitude is significantly reduced to less than 0.5 dB over 90% of the filter FSR.

Thanks to the optical phase control function in the FD-OP, the notch frequency of the primary and secondary tap distribution based MPNF can be continuously tuned by designing the phase shift of the *n*th secondary tap to be

$$\Delta\phi_{S,n} = (2n-1)\theta \tag{9}$$

where θ is the phase shift added to the first secondary tap. The filter *k*th harmonic notch frequency is given by

$$f_{\text{notch},k} = \frac{\pi(2k-1)+\theta}{\Delta\lambda D\pi}. \tag{10}$$

This shows the filter notch frequency is dependent on the dispersion parameter of the dispersive medium D and θ, which can be controlled by the FD-OP. For an illustration of the notch

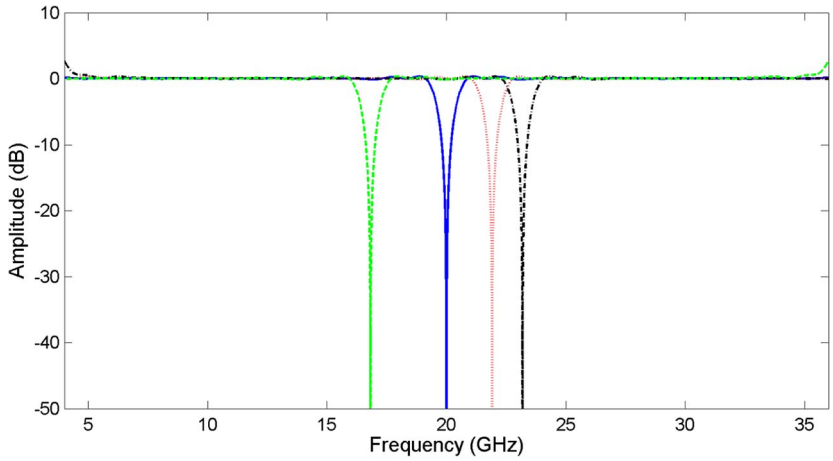

Fig. 6. Simulated tunable notch filter responses for $\theta = -0.5$ rad (dashed line), 0 rad (solid line), 0.3 rad (dotted line), and 0.5 rad (dot-dash line).

frequency tuning operation, the notch frequency is tuned from 16.9 GHz to 23.2 GHz by using different values of θ, as shown in Fig. 6.

It can be seen from the figure that by changing the θ values from 0 to -0.5, 0.3 and 0.5 rad, the notch frequency is tuned from 20 GHz to 16.9 GHz, 21.9 GHz, and 23.2 GHz, respectively. Since θ can be any value between $-\pi$ to π rad by controlling $\Delta\phi_{S,n} = \phi_{cS,n} - \phi_{sS,n}$, the filter notch frequency can be continuously tuned over the full FSR. Note that while tuning the notch frequency, the notch width and the FSR of the notch filter remain unchanged. This shows the advantage of the novel optical phase control notch frequency tuning technique compared to the conventional technique that uses a wavelength tunable laser and a wavelength dependent time delay element to change the fundamental time delay of the structure, which alters not only the notch frequency but the response shape as well.

The primary and secondary tap distribution based MPNF has a simple structure. It does not involve any electrical components and hence it can be operated in microwave and even millimeter wave frequency range. The bandwidth of the primary and secondary tap distribution based MPNF is only limited by the optical phase modulator bandwidth. A 100-GHZ-bandwidth electro-optic modulator has been reported [19]; therefore, the notch filter can operate to at least 100 GHz. Using an optical phase modulator has the advantage of no DC bias voltage required and no bias drift problem, which is presented in the conventional fiber optic links and many reported MPNFs that use an optical intensity modulator for RF signal modulation. The primary and secondary tap distribution based MPNF does not suffer from the problems of high output noise power and environmental sensitive response performance, which are presented in the conventional IIR structure based microwave photonic filters and the SBS based filters. For example, the SBS based filters presented in [10] and [11], which have a narrow notch and the continuous notch frequency tunability, require careful control of the light polarization state into the SBS medium to realize a deep notch and have a frequency response shape that depends on the input RF signal power. Such problems are not presented in the primary and secondary tap distribution based MPNF.

4. Experimental Results

An experiment was set up as shown in Fig. 7 to verify the proof of principle for the primary and secondary tap distribution based MPNF. A C-band wavelength tunable laser, which has a narrow linewidth of < 100 kHz and a maximum 16 dBm output optical power, was used as the primary source. An FP laser, which was operated at around 1550 nm and had a wavelength separation between adjacent modes of 1.26 nm, was used as the secondary source. The FP laser was followed by an optical filter that selected the six wavelengths at the center of the FP laser

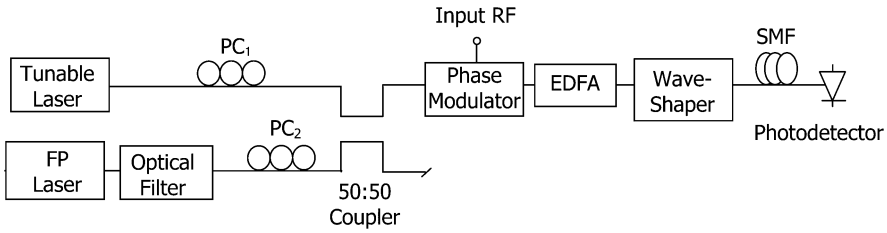

Fig. 7. Experimental setup of the primary and secondary tap distribution based MPNF.

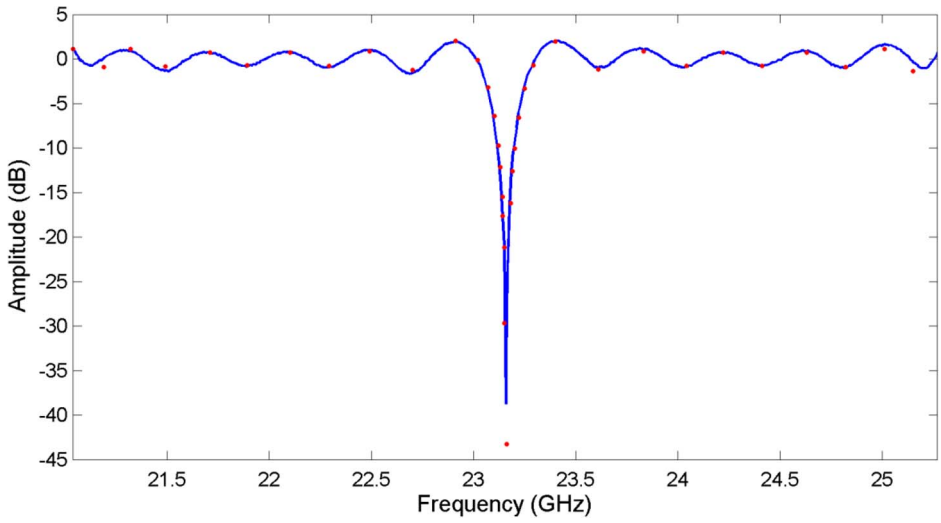

Fig. 8. Measured (solid) and simulated (dots) responses of the primary and secondary tap distribution based MPNF.

spectrum. The wavelength of the tunable laser was tuned to be 0.63 nm away to the left of the first secondary wavelength in order to satisfy the filter tap time delay requirement. The primary and secondary source were combined by a 50:50 optical coupler and were modulated by a 40 GHz bandwidth optical phase modulator. A polarization controller (PC) was used after the tunable laser and the FP laser to align the light polarization state to maximize the phase modulator efficiency. The PCs can be avoid by using polarization maintaining components between the laser sources and the phase modulator. The different-wavelength RF phase modulated optical signals were amplified by an erbium-doped fiber amplifier (EDFA) and launched into an FD-OP (Finisar WaveShaper 4000s), which was programmed to eliminate the lower sidebands and to set the phase and the amplitude of the different wavelength optical carriers and upper sidebands to the desired values. The processed RF phase modulated optical signals passed through a 20-km-long single mode fiber (SMF) with a dispersion parameter of 17 ps/km $\cdot$ nm and was detected by a 50 GHz bandwidth photodetector connected to a 26.5 GHz bandwidth network analyzer to display the filter frequency response.

The FD-OP was programmed to equalize the secondary tap amplitude and to set the amplitude of the primary tap to be the sum of the secondary tap amplitudes. The frequency response was measured as shown in Fig. 8. The simulated response obtained using (7) together with the experimental parameters is also shown in the figure for comparison. Excellent agreement between the experimental measurement and the theoretical prediction can be seen. Over 40 dB notch depth was obtained at the microwave frequency of 23.16 GHz. The filter FSR was 4.69 GHz determined by the wavelength separations and the length of the SMF, which generated a time delay of 0.214 ns. The filter FSR can be increased by using a using a shorter fiber as the dispersive medium or reducing the wavelength separations. There were around 3 dB ripples over the

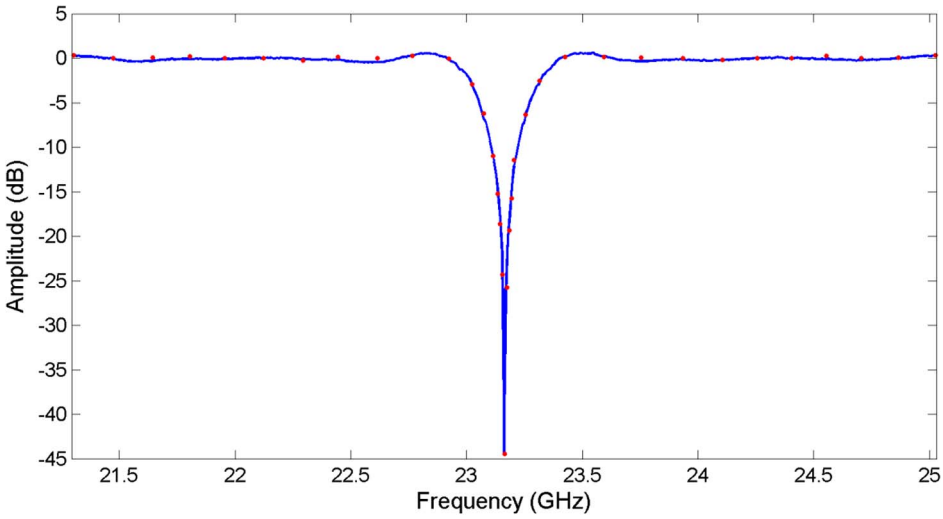

Fig. 9. Measured (solid) and simulated (dots) responses of the primary and secondary tap distribution based MPNF with the secondary tap amplitudes designed to minimize the passband ripples.

operating range that encompassed most of the FSR. In order to reduce the filter passband ripples, the amplitude ratios of the secondary taps were designed to be 1, 0.85, 0.7, 0.45, 0.3, and 0.15, and the primary tap amplitude ratio of 3.45, which was the sum of all the secondary tap amplitude ratios, was used in the experiment. Fig. 9 shows a comparison between the measured and predicted frequency responses of the notch filter with optimum designed tap amplitudes. Again, excellent agreement between the experimental measurement and the theoretical prediction can be seen. The ripples in the notch filter passband have been reduced to around 1 dB over the operating range which is 84% of the filter FSR. The notch filter response shown on the network analyzer was very stable with the notch depth of > 40 dB.

The signal-to-noise ratio (SNR) of the novel all-optical MPNF was measured to be 114.3 dB/Hz for an input RF signal power of 5 dBm into the phase modulator and an output optical power of 0 dBm into the photodetector. The signal-spontaneous beat noise from the EDFA and the laser intensity noise from the FP laser were found to be the dominant noise sources. The filter SNR can be increased by using a high-power secondary source with low relative intensity noise.

Continuous notch frequency tuning was demonstrated by controlling the phases of different-wavelength optical carriers and sidebands according to (9) via the FD-OP. The measured continuously tunable notch filter response is shown in Fig. 10. The notch frequency was tuned from 23.68 GHz to 23.29 GHz and 24.08 GHz by changing the value of θ from 0 rad to -0.51 rad and 0.53 rad and agrees with (10). The notch depth of > 40 dB was maintained while tuning the notch frequency. The -6 dB notch width, as well as the FSR of the notch filter, remained the same when the notch frequency tuned. This shows the advantage of controlling the phase shift compared to changing the fundamental time delay, which was used in most of the reported tunable MPNFs, to tune the notch frequency as it does not affect the notch filter frequency response shape. Note that only three tunable notch filter responses with $\theta = -0.51$, 0, and 0.53 rad are shown in Fig. 10. Since the phase shift θ added to the first secondary tap can be any value between $-\pi$ and π rad by controlling the FD-OP, the notch frequency can be tuned over the full FSR.

The resolution of the FD-OP used in the experiment is 12 GHz, which limits the system lowest operating frequency. However, it should be noted that there are strong and ongoing driving forces to increase the LCoS resolution that come from important consumer electronics applications such as TV and projection systems, 3-D imaging and defense. Significantly higher resolution has been reported from commercially available 2-D LCoS displays that can support an increased number of 1920 $\times$ 1080 pixels with a reduced pixel size down to 8 μm [20].

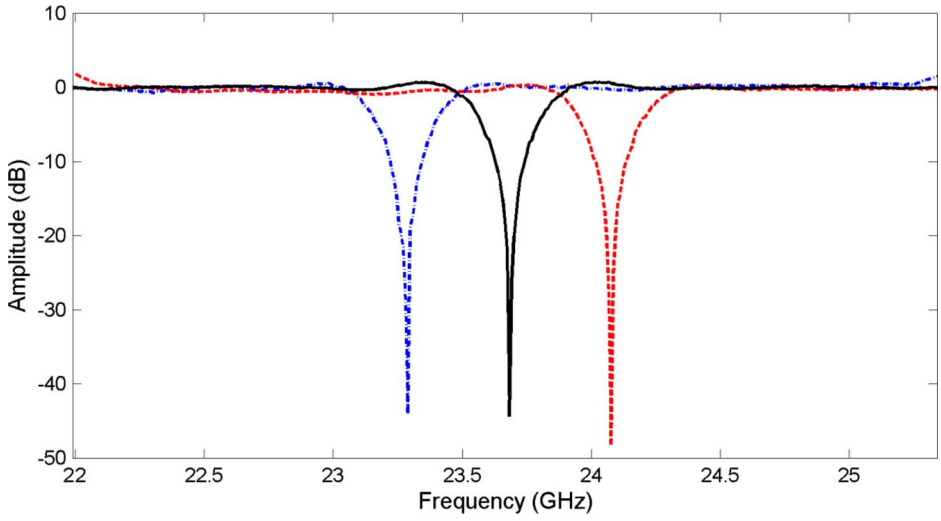

Fig. 10. Measured tunable notch filter responses for $\theta = -0.51$ rad (dot-dash line), 0 rad (solid line), and 0.53 rad (dashed line).

Meanwhile, due to the recent advancement in technology and strong demand in consumer electronic applications, the cost of the LCoS array, which is the main component of the FD-OP, has significantly reduced. For example, the cost of an LCoS-based pico projector is only around $\$100$.

5. Conclusion

A new continuously-tunable MPNF that can realize a flat and wide passband, as well as a large FSR frequency response, has been presented. It is based on designing the filter impulse response to have a primary and secondary tap distribution, where the primary tap amplitude is the sum of all the secondary tap amplitudes and the separation of the primary tap to the first secondary tap is half the adjacent secondary taps separation. The MPNF has the ability to realize high resolution filtering by using the optical source such as a wide-band parametric frequency comb generator that has the ability to generate many wavelengths as the secondary source. The primary and secondary tap distribution-based MPNF does not require DC bias voltage and is free of the bias drift problem as an optical phase modulator is used for RF signal modulation. It does not suffer from the input RF signal power dependent frequency response problem, which is presented in the SBS based microwave photonic filters. Experimental results have demonstrated the MPNF, exhibiting a large FSR, a flat passband of < 1 dB ripple, and a deep notch of > 40 dB. The continuous notch frequency tuning operation has also been demonstrated by controlling the phase shift of the secondary taps via a diffraction-based Fourier-domain optical processor.

References

[1] R. A. Minasian, E. H. W. Chan, and X. Yi, "Microwave photonic signal processing," *Opt. Exp.*, vol. 21, no. 19, pp. 22 918–22 936, Sep. 2013.
[2] W. Li, N. Zhu, and L. Wang, "Continuously tunable microwave photonic notch filter with a complex coefficient," *IEEE Photon. J.*, vol. 3, no. 3, pp. 462–467, 2011.
[3] C. Zhang *et al.*, "A tunable microwave photonic filter with a complex coefficient based on polarization modulation," *IEEE Photon. J.*, vol. 5, no. 5, Oct. 2013, Art. ID. 5501606.
[4] Y. Zhang and S. Pan, "Complex coefficient microwave photonic filter using a polarization-modulator-based phase shifter," *IEEE Photon. Technol. Lett.*, vol. 25, no. 2, pp. 187–189, Jan. 2013.
[5] E. H. W. Chan and R. A. Minasian, "Coherence-free equivalent negative tap microwave photonic notch filter based on delayed self-wavelength conversion," *IEEE Trans. Microw. Theory Techn.*, vol. 58, no. 11, pp. 3199–3205, 2010.
[6] X. Li *et al.*, "Microwave photonic filter with multiple taps based on single semiconductor optical amplifier," *Opt. Commun.*, vol. 283, no. 15, pp. 3026–3029, Aug. 2010.

[7] X. Wang, E. H. W. Chan, and R. A. Minasian, "Microwave photonic notch filter based on a dual-Sagnac-loop structure," *Appl. Opt.*, vol. 49, no. 33, pp. 6546–6551, Nov. 2010.
[8] E. H. W. Chan and R. A. Minasian, "Multiple-tap, tunable microwave photonic interference mitigation filter," *J. Lightw. Technol.*, vol. 29, no. 8, pp. 1069–1076, Apr. 2011.
[9] R. Tao, X. Feng, Y. Cao, Z. Li, and B. Guan, "Tunable microwave photonic notch filter and bandpass filter based on high-birefringence fiber-Bragg-grating-based Fabry–Perot cavity," *IEEE Photon. Technol. Lett.*, vol. 24, no. 20, pp. 1805–1808, Oct. 2012.
[10] W. Zhang and R. A. Minasian, "Ultra-wide tunable microwave photonic notch filter based on stimulated Brillouin scattering," *IEEE Photon. Technol. Lett.*, vol. 24, no. 14, pp. 1182–1184, Jul. 2012.
[11] D. Marpaung, B. Morrison, R. Pant, and B. J. Eggleton, "Frequency agile microwave photonic notch filter with anomalously high stopband rejection," *Opt. Lett.*, vol. 38, no. 21, pp. 4300–4303, Nov. 2013.
[12] W. Li, L. X. Wang, and N. H. Zhu, "All-optical microwave photonic single-passband filter based on polarization control through stimulated Brillouin scattering," *IEEE Photon. J.*, vol. 5, no. 4, Aug. 2013, Art. ID. 5501411.
[13] X. Zou, W. Li, W. Pan, L. Yan, and J. Yao, "Photonic-assisted microwave channelizer with improved channel characteristics based on spectrum-controlled stimulated Brillouin scattering," *IEEE Trans. Microw. Theory Techn.*, vol. 61, no. 9, pp. 3470–3478, Sep. 2013.
[14] M. Pagani, E. H. W. Chan, and R. A. Minasian, "A study of the linearity performance of a stimulated Brillouin scattering-based microwave photonic bandpass filter," *J. Lightw. Technol.*, vol. 32, no. 5, pp. 999–1005, Mar. 2014.
[15] M. A. F. Roelens *et al.*, "Dispersion trimming in a reconfigurable wavelength selective switch," *J. Lightw. Technol.*, vol. 26, no. 1, pp. 73–78, Jan. 2008.
[16] J. L. Corral, J. Marti, J. M. Fuster, and R. I. Laming, "Dispersion induced bandwidth limitation of variable true time delay lines based on linearly chirped fiber gratings," *Electron. Lett.*, vol. 34, no. 2, pp. 209–211, Jan. 1998.
[17] X. Feng, H. Tam, H. Liu, and P. K. A. Wai, "Multiwavelength erbium-doped fiber laser employing a nonlinear optical loop mirror," *Opt. Commun.*, vol. 268, no. 2, pp. 278–281, Dec. 2006.
[18] V. Ataie, E. Myslivets, B. P.-P. Kuo, N. Alic, and S. Radic, "Spectrally equalized frequency comb generation in multi-stage parametric mixer with nonlinear pulse shaping," *J. Lightw. Technol.*, vol. 32, no. 4, pp. 840–846, Feb. 2014.
[19] H. Huang *et al.*, "Broadband modulation performance of 100-GHz EO polymer MZMs," *J. Lightw. Technol.*, vol. 30, no. 23, pp. 3647–3652, Dec. 2012.
[20] F. Yaras, H. Kang, and L. Onural, "State of the art in holographic displays: A survey," *J. Display Technol.*, vol. 6, no. 10, pp. 443–454, Oct. 2010.